Scientific Justification

Pox 186 is an extraordinary, nearby (D∼18 Mpc) starbursting dwarf galaxy. It is remarkable, if not unique, in that it is hosting a dominant burst of star-formation, yet it is undetected in HI 21-cm emission. Typically, starbursting dwarf galaxies have large HI reservoirs (e.g., Thuan et al. 2016), where the HI mass dominates the stellar mass, but for Pox 186, the non-detections limit the HI/L_B ratio to a factor of many times smaller than typical dwarfs (Thuan et al. 1987). How did Pox 186 arrive at this stage? A likely explanation is that the starburst was energetic enough to drive away all of the neutral ISM. This scenario is supported by the observation of outflows evidenced by broad wings (FWHM$\sim 800\,\mathrm{km\,s^{-1}}$) in its [O III] emission lines. In theory, it is energetically possible for a starburst to drive away its entire ISM, but there are no galaxies where this has been unambiguously observed. If this is the case, then it is likely that Pox 186 is leaking a very large fraction of its Lyman continuum (LyC) emission, potentially the strongest low-z LyC emitter. Thus, Pox 186 is a nearby, resolved analog to the high redshift systems that are held responsible for the reionization of the universe.

We propose to observe Pox 186 to secure the interpretation as a case of complete neutral gas blow-away, and to study its tracers of LyC emission. With broad-band and narrow-band imaging, we will test if the ionization structure is consistent with a density bounded geometry that would be the result of a neutral gas blow away. Additionally, we will map the Mg II emission through imaging which has recently been proposed as a tracer of the fractional escape of LyC emission (Henry et al. 2018). Finally, we will obtain a COS spectrum to study the gas outflow and the properties of the stars responsible for the intense feedback.

Pox 186 as an Analog: Recently, it has become clear that low mass star-forming galaxies are the primary sources of ionizing photons during the epoch of reionization (but see Naidu et al 2019 for a different view). A galaxy's capacity to contribute to reionization depends on its total ionizing flux and the fraction ($f_{\rm esc}$) that escapes its interstellar medium (ISM) and circumgalactic medium, reaching the intergalactic medium (IGM). For reionization to be complete by z∼6, *all galaxies* must have had an average escape fraction between 10-20% (Robertson et al. 2015; Finkelstein et al. 2015), or the ionizing photon production efficiency must be higher than previously assumed (Finkelstein et al. 2019). Direct observations of the escaping ionizing flux from these galaxies is difficult due to an increasingly opaque IGM beyond $z > 4$. Therefore analogs at lower redshift are sought to provide insight into environments that promote higher $f_{\rm esc}$.

Typical galaxies at lower redshift have $f_{\rm esc}$ on the order of a few percent, but a population with high escape fractions has been found, the Green Peas (GPs, Cardamone et al. 2009). Selected for their high [O III]/[O II] (O_{32}) ratio, GPs are compact, highly star-forming galaxies with characteristics similar to those responsible for reionization. Some GPs have LyC escape fractions as high as 70% (Izotov et al. 2016a,b; Schaerer et al. 2016; Verhamme et al. 2017) and a strong anti-correlation between the separation of Lyman alpha peaks and $f_{\rm esc}$ has been observed (Izotov et al. 2018b), implying gas kinematics and structure play an important role in determining $f_{\rm esc}$. However, GPs are limited as useful analogs as they are many times more

massive than the galaxies responsible for reionization (e.g., Weisz & Boylan-Kolchin 2017) while simultaneously being too compact and far away (z∼0.3) to be structurally studied in detail. Local (z≈0) analogs have been sought to bridge this gap. One such analog is Mrk 71, which has been studied in detail (Micheva et al. 2017). A luminous H II region with properties similar to the GPs but in a galaxy with a luminosity two orders of magnitude fainter, used as a laboratory of a nearby LyC leaker. Mrk 71, however, is still not a perfect analog because it resides inside a larger host galaxy (NGC 2366). Pox 186 is unique in allowing for the mapping of gas structure in an entire galaxy with properties analogous to GPs, but a mass similar to galaxies responsible for reionization, enabling a more fundamental understanding of both populations individually and how they compare.

Pox 186 as a local LyC leaker: Multiple observations indicate that Pox 186 may be *globally* ionized by its current star-formation episode. First, Guseva et al. (2004) measure a O_{32} emission line ratio of ∼22, ranking Pox 186 among the most extreme Blue Compact Dwarfs (BCDs) and GPs observed. High values of O_{32} have been suggested to be an indicator of density-bounded H II regions (Jaskot & Oey 2013; Jaskot et al. 2017; Izotov et al. 2017). Second, the inferred S/O abundance ratio is ∼2 times larger than the mean for BCDs. This abundance is most easily understood if the H II region is density-bounded and inappropriate ionization corrections, which are derived from ionization-bounded H II region models, are used (Guseva et al. 2004). Third, Pox 186 is not detected in HI, despite multiple attempts (Kunth et al. 1988, Begum et al. 2005). With a 5σ upper limit of 1.6×10^6 $M_\odot$ in HI, its M_{HI}/L_B ratio is much lower than that for typical BCDs. When combined with the M_{HI} expected from its dust content (Izotov et al. 2014, 2×10^8 $M_\odot$), these measurements suggest that a large portion of the HI has been ionized. As a reference, NGC 2366, the host galaxy of Mrk 71 mentioned above, has a total HI mass of 6×10^8 $M_\odot$ (van Eymeren et al. 2008).

Existing data do not tell us anything about the structure of the ionized region, as seeing-limited ground based observations are not sufficient to resolve it (Figure 1). Pox 186 is extremely compact and HST is required to perform resolved studies. At a redshift of 0.004, Pox 186 is too close for a direct detection of LyC radiation, due to absorption by galactic HI. Thus, in order to study the ionizing output of this remarkable galaxy, we need to resort to indirect indicators. **Specifically, we propose to use images of low- and high-ionization oxygen lines to map Pox 186's ionizing structure, as well as images of Mg II emission lines, to detect the presence of residual neutral gas.**

Maps of O_{32}: Pellegrini et al. (2012) showed that mapping the ionization parameter (e.g., via O_{32}) can help diagnose density-bounded optically thin nebulae. For radiation-bounded H II clouds, the [O III] emitting region will be surrounded by the lower ionization [O II]. Micheva et al. (2017) showed that knot A in Mrk 71 is surrounded by a low-ionization zone in all directions except for a ruptured part to the north. This morphology indicates that LyC radiation is escaping through the broken bubble. Only Hubble will allow the angular resolution necessary to conduct a similar analysis of Pox 186. Using the [O III] and [O II] narrowband filters, we will map the ionization structure of Pox 186 on scales of ∼ 10pc (corresponding to 0.″1). Hβ and Hα observations are also required to map the dust extinction.

Tracing the ionizing radiation with nebular Mg II: Henry et al. (2018) discovered a

tight correlation between the escape fraction of Lyα and Mg II photons in GP galaxies. It stands to reason that the intensity of the two lines are related, as both Mg II and Lyα are resonant transitions, and Mg^+ ions, responsible for the scattering of the Mg II line, are co-spatial with the neutral hydrogen gas responsible for the scattering of the Lyα photons (Finley et al. 2017; Henry et al. 2018). We expect that a LyC emitter will show Mg II in emission co-spatial with the other emission lines produced in the H II region. Photoionization modeling demonstrates that the O_{32} ratio can be used to predict the expected Mg II output for a variety of ionization conditions and gas metallicities (Henry et al. 2018).

We will use the O_{32} line ratio maps to predict the expected surface brightness distribution of the Mg II emission. The comparison between the measured and predicted maps will then give us crucial information about the amount of scattering the Mg II photons experienced, and thus, the amount of neutral gas along the line of sight. This is a new and unexplored diagnostic, with the potential to be used as a LyC indicator in galaxies at $z > 6$. Our proposed observations will enable us to resolve this emission for the first time, and link it to the optically-thin regions identified in the O_{32} maps.

Characterizing feedback with COS: The presence of high velocity wings seen in the [O III] lines (Fig 2) suggests a multi–phase outflow, in which the observed wings result from mixing between a hot wind and cooler gas clouds (Schneider et al. 2020). Recent studies show that these hot winds can create highly ionized channels, that enhance the escape of ionizing radiation (e.g., Jaskot et al. 2019). With the proposed COS spectrum we will simultaneously study the outflow (through the absorption lines) and the stars producing the energy that is driving it (through the continuum and emission lines).

The proposed UV spectrum will cover crucial resonant transitions in low and high ionization metals (Si II, Si IV, and C IV), which probe outflowing gas in a range of temperatures ($10^4 < T < 10^5$K). Modeling their relative strengths and absorption line profiles will constrain the velocity, density, and temperature structure of the outflowing gas (e.g., Carr et al. 2018, Chisholm et al. 2018, Schneider et al. 2020). Additionally, we will model the stellar continuum together with any nebular detected emission line (e.g., HeII, C IV, OIII]) to constrain the age and metallicity of the hottest stars, as well as their ionizing output.

Resolved stellar population analysis: HST WFPC2 observations revealed the presence of a complex morphology in the central 1.″0 region of Pox 186 (Corbin & Vacca 2002). Figure 1 shows an extremely compact star forming clump, $\leq$ 120 pc in radius, surrounded by an irregular structure and a tail. This image was taken with the F555W filter which includes the emission from the very bright [O III] line. Subsequent long-slit spectra showed that strong nebular emission lines contribute substantially to the broad band image (Guseva et al. 2004). Thus the irregular structure could be due to gas photoionized by radiation escaping from the central star-burst (e.g., similar to Mrk 71). We will separate the nebular and stellar components, on scales small enough to resolve the central region and use resolved SED fitting to interpret the stellar continuum maps from the rest-frame UV to the optical. The modeling will result in maps of star-formation history, stellar mass, and star-formation rate, which will be used to estimate the intrinsic ionizing radiation field being produced by Pox 186 and directly measure the feedback from the central star cluster.

Description of the Observations

We request WFC3/UVIS imaging of Pox 186 with 5 narrow, 2 medium, and 2 broad-band filters, and a COS spectrum with the G160M grating. Specifically, we allot 1.5 orbits of time in both the F280N and F373N filters, 1 orbit for F487N, and $\frac{1}{2}$ an orbit for each of the remaining: F502N, F658N, F621M, F467M, F336W and F225W. For the G160M spectrum we allot 4 orbits.

Why HST. Detailed analysis of the properties of the ISM, its ionization state, and the geometry of the gas in Pox 186 requires the UV capabilities only available through HST. Moreover, the high angular resolution required for the proposed scientific analysis is far more challenging to achieve from the ground.

Measuring the Emission Line Maps. We will measure spatial emission line maps for Pox 186 using a combination of narrow band filters centered on the emission lines and broad-band measurements of the continuum in the vicinity of the lines. Table 1 shows our proposed filter combinations and exposure times while Figure 3 shows how these filters fall on Pox 186's spectrum. Our continuum filters (F225W, F336W, F467M, and F621M) sample the full optical spectrum and NUV. They are chosen to avoid any strong nebular lines such that they can be used to isolate the emission lines as measured by the narrow-bands *and* be used to measure the stellar continuum without ionized gas contaminating the measurement.

Our exposure times are set to detect the surface brightness emission at a distance of $1\farcs0$ from the center with a S/N of 3 per resolution element. In the external regions, the resolution element is set to $0\farcs2\times0\farcs2$, it will be smaller towards the center where the surface brightness increases. We use the Gemini emission line profiles to estimate the line flux surface brightnesses finding: 2×10^{-16}, 9.91×10^{-17}, 4.5×10^{-15}, and 2.75×10^{-15} c.g.s/arcsec^2 in the [O II], Hβ, [O III] and Hα lines, respectively. We estimate the Mg II emission line flux based on photoionization models from the [O III]/[O II] ratio from Guseva et al. (2004) and the measured [O III] flux. We predict Mg II flux of 1×10^{-15} c.g.s./arcsec^2.

Using the ETC we find that we require an exposure time of 4,150 seconds to reach a S/N of 3 per resolution element in the Mg II line. Similarly, we need an exposure time of 5500 seconds to reach a S/N of 5 in the [O II] line. The total integration time will be split over 3 dithered frames to mitigate the impact of cosmic rays. A post flash ranging from 8-12e$^-$ per pixel is chosen for the various filters to best mitigate the effect of charge transfer efficiency degradation.

PSF Matching. HST's PSF changes marginally over the range of wavelengths covered by the proposed observations. However, in order to make accurate line ratio and color maps for our target, we will need to carefully treat even the minor changes in the PSF. We will use the stars present in our field of view to complement the TinyTim models in order to generate an accurate PSF for each of our filters. Using these, we will compute a kernel that will allow us to homogenize the PSF across the various filters. This will be done as the first step before any analysis in order to ensure that we consider the same regions of the galaxy when making inferences using information from different filters.

COS Observations. At $z = 0.004087$, G160M covers absorption lines from many

Spectral feature	Filter	Orbits	Post-flash
Mg II $\lambda\lambda$2796,2803	F280N	1.5	12e$^-$
[O II] λ3727	F373N	1.5	8 e$^-$
Hβ λ4861	F487N	1.0	11e$^-$
[O III] $\lambda\lambda$4959,5007	F502N	0.5	11e$^-$
Hα λ6563	F658N	0.5	12e$^-$
Continuum	F621M	0.5	12e$^-$
Continuum	F467M	0.5	12e$^-$
Continuum	F225W	0.5	12e$^-$
Continuum	F336W	0.5	12e$^-$

Table 1: The requested exposure times for the proposed filters.

Absorption line feature	Wavelength (Å)	Ionization Energy (eV)
Si II	1526	8.2
Si IV	1393,1402	33.5
C IV	1548,1550	47.9

Table 2: Absorption lines covered by the requested observations

ionization species shown in Table 2, with a resolution of $R = 15000$ (i.e., $20\,\mathrm{km\,s^{-1}}$). At this resolution the absorption lines, which we expect to have widths larger than a few hundred $\mathrm{km\,s^{-1}}$ will be well sampled even after binning 2 resolution elements (12 pixels in the dispersion direction). Based on previous experience we need a S/N = 10 per resolution element in the continuum in order to study absorption line profiles. We estimate the exposure time to reach the required S/N assuming a flat continuum in f_ν, a flux normalization of 3.6×10^{-16} c.g.s based on archival F336W data, and a 2 resolution element binning strategy. We find we need 10,800 seconds to reach a S/N = 10 per $40\,\mathrm{km\,s^{-1}}$ resolution element. The ETC ID is COS.sp.1430070. Assuming target acquisition and overheads take an additional 150 seconds, we request 4 COS orbits.

Observing Plan. To observe 9 different filters, each with 3 frames, in 7 orbits while maximizing the S/N of the emission lines, we propose grouping the exposures in the following way. [O II] plays a central role in our science goals and thus will demand the most exposure time. Combining F373N with F621M, which only needs 500 seconds to reach a SN of 22.8 per binned pixel, will allow us to dedicate 5500 seconds to the 3 exposures in F373N. Likewise, grouping F280N and F336W across 2 orbits with exposure times of 5500 seconds and 500 seconds respectively reaches S/N levels of 3.89 for F280N and 13.1 for F336W. 1500 seconds, or half an orbit, for F225W, F467M, F502N, and F658N reaches a S/N of 20.35, 28.49, 19.57, and 13.017 respectively. Finally with the last orbit we propose to observe F487N for 3000 seconds which gives a S/N of 6.53.

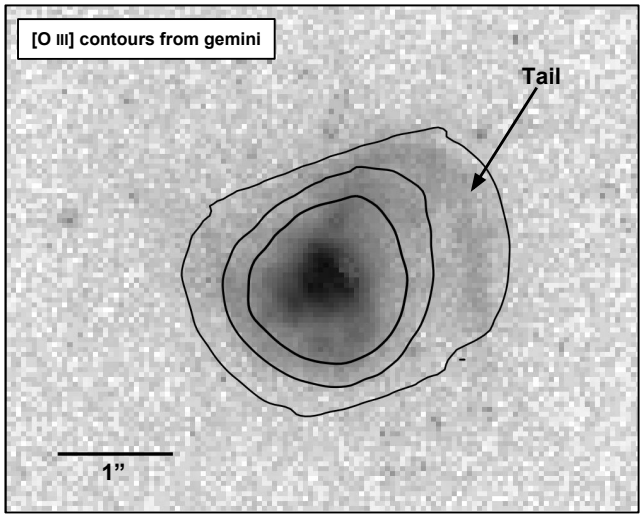

Figure 1: **Resolving the small scale structure of Pox 186 from the ground is challenging, and the UV cannot be observed.** This figure shows an existing HST WFPC2 F555W image of Pox 186 in greyscale with [O III] emission from Gemini IFU data overlaid as contours. Clearly, ground-based optical imaging is inadequate to map the resolved ionization structure of Pox 186. While the Gemini observations have high S/N ratios ($\geq$ 20), the higher angular resolution of HST is required to make emission line ratio maps. It is worth highlighting that the light in the F555W is dominated by the [O III] emission.

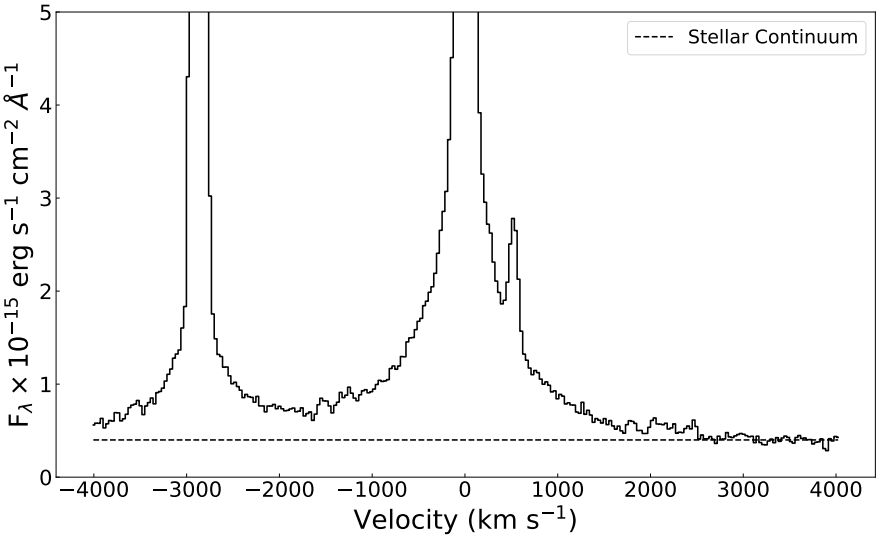

Figure 2: **The wings of the [O III] lines show gas moving $>$ 1,000 km s^{-1}.** Gemini IFU observations show broad line emission at the base of the [O III] lines. (The faint narrow line is due to He I 5016.) These broad wings can result from the mixing between a hot moving wind and cold clouds being transported outward. The proposed COS spectrum will test this model directly by probing gas with temperatures between 10^4 and 10^5K.

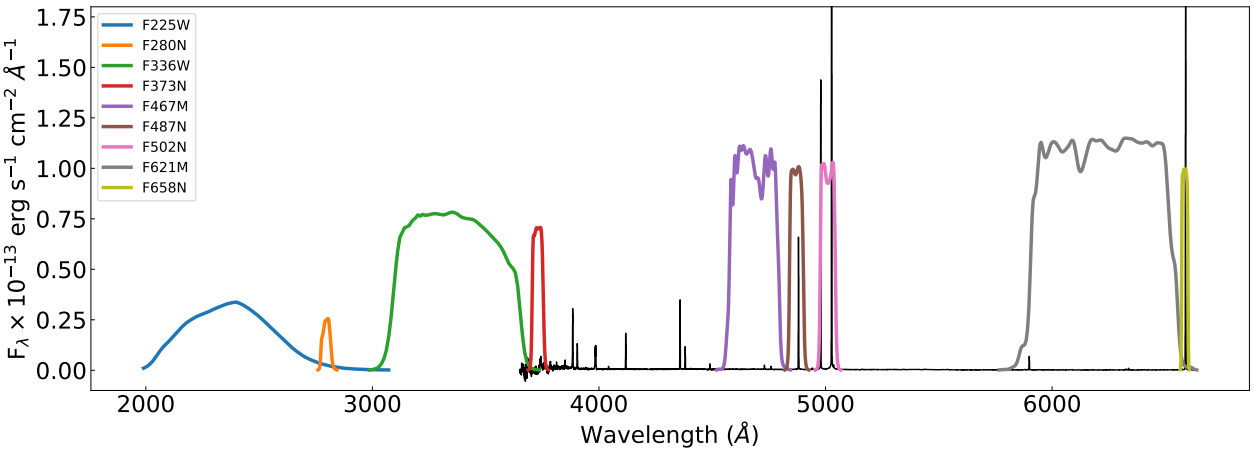

Figure 3: **The proposed filter set will probe both the nebular and stellar continuum.** This figure shows the selected WFC3/UVIS filters along with the Pox 186 optical spectrum (*black*). The optical spectrum is from Gemini IFU data, extracted from the central 1.″5. The filter transmission curves have been scaled to better show their overlap with the emission lines. The narrow-band filters isolate important emission lines. The broadband filters have been chosen to allow for accurate continuum subtraction from the narrowband images and will allow an uncontaminated comparison of the stellar and gaseous distributions. **Only with HST we can acquire the required NUV high spatial resolution data.**

Special Requirements

N/A

Coordinated Observations

N/A

Justify Duplications

HST obtained WFPC2 images (F336W, F555W, and F814W) and STIS UV spectroscopy (G140L and G230L) under GO-8333 (PI:Corbin). Our proposed observation in F336W may be considered as a duplication. We are re-observing the galaxy in this filter in order to have all exposures on the same pixel scales, to have an optimized dither pattern for *all* the bands, and to avoid large interpolations due to different rotations. The STIS spectra, published in Corbin & Vacca (2002), are too low S/N to be useful for our purposes.

References

Begum, A., & Chengalur, J. N. 2005, MNRAS, 362, 609
Cardamone, C., Schawinski, K., Sarzi, M., et al. 2009, MNRAS, 399, 1191
Carr, C., Scarlata, C., Panagia, N., & Henry, A., 2018, ApJ, 860, 143
Chisholm, J., Tremonti, C., Leitherer, C., 2018, MNRAS, 487, 1690
Corbin, M. R., & Vacca, W. D. 2002, ApJ, 581, 1039
Doublier, V., Kunth, D., Courbin, F., & Magain, P. 2000, A&A, 353, 887
Finkelstein, S. L., Ryan, R. E., Jr., Papovich, C., et al. 2015, ApJ, 810, 72
Finkelstein, S. L., D'Aloisio, A., Paardekooper, J. P., et al. 2019, ApJ, 879, 36
Finley, H., Bouché, N., Contini, T., et al. 2017, A&A, 608, A7
Guseva, N. G., Papaderos, P., Izotov, Y. I., et al. 2004, A&A, 421, 519
Henry, A., Berg, D. A., Scarlata, C., Verhamme, A., & Erb, D. 2018, ApJ, 855, 96
Izotov, Y. I., Guseva, N. G., Fricke, K. J., Krügel, E., & Henkel, C. 2014, A&A, 570, A97
Izotov, Y. I., Orlitová, I., Schaerer, D., et al. 2016a, Nature, 529, 178
Izotov, Y. I., Schaerer, D., Thuan, T. X., et al. 2016b, MNRAS, 461, 3683
Izotov, Y. I., Thuan, T. X., & Guseva, N. G. 2017, MNRAS, 471, 548
Izotov Y. I., Worseck G., Schaerer D., Guseva N. G., et al. 2018b, MNRAS, 478, 4851
Jaskot, A. E., & Oey, M. S. 2013, ApJ, 766, 91
Jaskot, A. E., Oey, M. S., Scarlata, C., & Dowd, T. 2017, ApJL, 851, L9
Jaskot, A. E., Dowd, T., Oey, M. S. Scarlata, C., & McKinney, J., 2019, ApJ, 885, 96
Kunth, D., Maurogordato, S., & Vigroux, L. 1988, A&A, 204, 10
Micheva, G., Oey, M. S., Jaskot, A. E., & James, B. L. 2017, ApJ, 845, 165
Naidu, R. P., Tacchella, S., Mason, C. A., et al. 2019, preprint (arXiv:1907:13130)
Pellegrini, E. W., Oey, M. S., Winkler, P. F., et al. 2012, ApJ, 755, 40
Robertson B. E., Ellis R. S., Furlanetto S. R., Dunlop J. S., 2015, ApJ, 802, L19
Schaerer, D., Izotov, Y. I., Verhamme, A., et al. 2016, A&A, 591, L8
Schneider, E. E., Ostriker, E. C., Robertson, B. E., Thompson, T. A., 2020 preprint (arXiv:2002.10468)
Thuan, T. X., 1987, in Nearly Normal Galaxies, ed. S. M. Faber (New York:Springer), 67
Thuan, T. X., Goehring, K. M., Hibbard, J. E., et al. 2016, MNRAS, 463, 4268
van Eymeren, J., Marcelin, M., Koribalski, B., et al. 2008, A&A, 493, 511
Verhamme, A., Orlitová, I., Schaerer, D., et al. 2017, A&A, 597, A13
Weisz, D. R., & Boylan-Kolchin, M. 2017, MNRAS, 469, L83